Static and Dynamic Photoelectrothermal Modeling of LED Lamps Including Low-Frequency Current Ripple Effects

Pedro S. Almeida, *Student Member, IEEE*, Vitor C. Bender, Henrique A. C. Braga, *Senior Member, IEEE*, Marco A. Dalla Costa, *Member, IEEE*, Tiago B. Marchesan, *Member, IEEE*, and J. Marcos Alonso, *Senior Member, IEEE*

***Abstract*—In this paper, a static and dynamic photoelectrothermal model including the impact of low-frequency current ripple on light-emitting diodes (LEDs) performance is proposed. The objective of this study is to evaluate the dynamical interaction among thermal, photometrical, and electrical properties of the LEDs when they are supplied by a dc constant current with a superposed low frequency sinusoidal ripple, which is the common case in offline LED drivers. Therefore, this paper presents both a model and experimental data for analyzing the LED photometrical behavior in terms of luminous flux, efficacy, flicker, and chromaticity. Three laboratory prototypes with different heat sinks and LED models have been tested. Experimental results are presented to evaluate the LED photometrical behavior under the aforementioned operating conditions and to validate the proposed modeling methodology.**

***Index Terms*—LED photometrical model, light-emitting diode (LED), light flicker, low-frequency current ripple, offline LED drivers.**

I. Introduction

NOWADAYS, light-emitting diodes (LEDs) are an attractive alternative for lighting under several perspectives. High luminous efficacy, robustness, long lifetime, high color rendering index (CRI), white light emission, and high reliability make them good candidates for applications on general indoor lighting, as well as being suitable for use in street lighting [1]–[3]. All these features make the white LED a good candidate to replace incandescent, fluorescent, and other discharge lamps in many applications [4].

Manuscript received April 4, 2014; revised May 27, 2014; accepted June 29, 2014. Date of publication July 17, 2014; date of current version February 13, 2015. This work was supported by the Brazilian Institutions Federal University of Santa Maria, Federal University of Juiz de Fora, FAPEMIG (Grant APQ 02401-12), and CAPES/DGU 249/11, and was also cosponsored by the Spanish government under Research grant DGPU PHB2010-0145-PC. Recommended for publication by Associate Editor S. Y. (R.) Hui.

P. S. Almeida and H. A. C. Braga are with the Federal University of de Juiz de Fora, Juiz de Fora 36036-330, Brazil (e-mail: pedro.almeida@engenharia.ufjf.br; henrique.braga@ufjf.edu.br).

V. C. Bender, M. A. Dalla Costa, and T. B. Marchesan are with the Federal University of Santa Maria, Santa Maria 97105-900, Brazil (e-mail: bender.vitor@gmail.com, madc.sm@gmail.com; tiago@gedre.ufsm.br).

J. M. Alonso is with the Department of Electrical Engineering, University of Oviedo, Oviedo 33003, Spain (e-mail: marcos@ieee.org).

Color versions of one or more of the figures in this paper are available online at http://ieeexplore.ieee.org.

Digital Object Identifier 10.1109/TPEL.2014.2340352

When LEDs are supplied from the ac power grid (50/60 Hz), the driving circuitry (e.g., the offline LED driver) imposes a current ripple on the LED at twice the line frequency (100/120 Hz). This oscillation is due to ac–dc conversion, and is usually filtered by the driving circuitry so as to deliver an almost constant current to the output; however, it cannot be entirely eliminated. Therefore, a sinusoidal current ripple (ac component) with a dc level is the waveform commonly found at the output of offline LED drivers. The LED current ac component may cause flicker, which is the cyclical variation of light in time, i.e., flicker is a modulation of light [5]. The human being is unable to directly perceive flicker perturbations with a frequency higher than the critical flicker frequency, which value is around 60–90 Hz. However, indirect perception of flicker is possible due to stroboscopic effects at frequencies of 100 Hz or higher (such as those generated by LED drivers) or fast eye motions (saccades). Thus, in these cases, the possible human perception needs to be taken into consideration [6].

Regarding the LEDs' supply, the Institute of Electrical and Electronics Engineers (IEEE) is preparing the PAR1789 recommended practice report for current modulation in LEDs for mitigating health risks to viewers [7]. Human biological effects are a function of flicker frequency, modulation depth, brightness, lighting application, and several other factors [7], [8]. Health effects such as headaches and eyestrain may occur after an exposure of several minutes to light flickering [7], [9].

In the case of analyzing the effects of LED current ripple, not only the flicker should be considered, but also the impact of the ripple current on the photometrical and colorimetrical performance of the LEDs. Effects such as degradation of flux and luminous efficacy with increasing current ripple amplitude, besides changes in chromaticity coordinates, CRI, and color-correlated temperature (CCT) occur due to inappropriate driving current waveform and poor thermal design [10]–[12].

The amount of current ripple is also an important electrical design constraint for LED drivers. The ac component amplitude of the output current waveform is inversely proportional to the amount of filtering capacitance used in the LED driver. For smaller ripples, bulkier capacitors are generally required.

The available range of capacitance values is largely dependent on capacitor type. For example, electrolytic capacitors, commonly used in power converters, present a low lifetime ($<$10 kh) when compared with LED themselves (50–100 kh). However, only the electrolytic technology is capable of

providing a greater range of capacitance values. Thus, seeking the reduction of capacitance is advantageous so as to replace this capacitor technology by, for example, polyester or polypropylene film technologies, which present a more compatible lifetime with LEDs. In this way, the LED driver lifespan may be extended. The reduction in the capacitive filter is an important topic of research and several methods have recently been proposed [13]–[18]. An acceptable increase in the LED current ripple may also provide a significant reduction in capacitances as long as maintenance of the LEDs performance, i.e., their light output can be assured [10], [19]–[21].

In this paper, the impact of the LED current ripple on its photometrical and colorimetrical properties is investigated. The photoelectrothermal behavior of the LED system will be analyzed for an LED current waveform composed by a dc current level and a superposed 120 Hz sinusoidal ripple.

The paper is organized as follows: Section II presents the static photoelectrothermal characterization, which takes into account only the effect of the dc current level. In Section III, the current ripple is taken into account in the analyses and the dynamical performance is evaluated. Section IV presents the experimental setup assembled to carry out practical tests. In Section V, the main conclusions extracted from this experimental work are highlighted.

II. Static Photoelectrothermal Model

Spectrophotometric quantities such as luminous flux, luminous efficacy, chromaticity coordinates, CRI, CCT, and flicker are substantially dependent on electrical properties (e.g., forward current and voltage) and thermal properties (e.g., junction temperature and thermal resistances). Therefore, the photometric analysis may not always be straightforward and these interactions need to be taken into account.

Previous studies [22]–[24] propose correlating the thermal, electrical, and photometrical aspects of LED systems by means of an integral model. In [22], the LED electrical behavior is obtained by a linear fitting of the curve given by forward voltage as a function of forward current, which is usually provided by LED manufacturers in the devices datasheet. It must be noted that this approach offers a good approximation at operating points within the linear portion of the LED characteristic, but will lack accuracy at lower current levels (close to the knee of the *I–V* curve). The dependent term of linear fitting represents the LED series resistance (R_s) and the independent term represents the LED threshold voltage (V_o). Since the LED voltage is also dependent on temperature, the rate of change in forward voltage (V_f) with the increase in the junction temperature (T_j), namely k_v, which is usually negative, must also be taken into account. Therefore, the LED electrical behavior taking k_v into account is then represented by (1), where I_f is the LED forward current, T_j is the junction temperature, and T_o is a reference temperature given in the datasheet [25]–[27]

$$V_f(I_f, T_j) = V_o + R_s I_f + k_v(T_j - T_o). \tag{1}$$

The thermal behavior of the system can be represented by *n* ideally identical LEDs placed on the same heat sink by a simplified thermal circuit, as the one shown in Fig. 1 [22], [24]. This figure shows both the electric and the thermal domains represented by means of circuit elements—the electrical domain side is a circuit representation of (1), with the linearized LED electrical model including effects of temperature on the LED voltage. At the thermal domain side, the node voltages actually represent the temperature at those points. From this circuit, both the heat sink temperature $T_{\rm hs}$ and the junction temperature T_j can be calculated. In (1) and (2), $R_{\rm hs}$ and $R_{\rm jc}$ represent the heat sink-to-ambient and junction-to-case thermal resistances, respectively, T_a is the ambient temperature, and k_h refers to the ratio of LED power that turns into heat to the LED radiant power. This parameter is given in the LED datasheet or otherwise, it could be obtained experimentally by measuring the LED electrical power and the radiant power. By combining (1)–(3), it is possible to find the terminal voltage V_f of each LED in the string of *n* LEDs, considering both electrical and thermal effects by $R_{\rm ja} = R_{\rm jc} + nR_{\rm hs}$. This electrothermal model is given by (4)

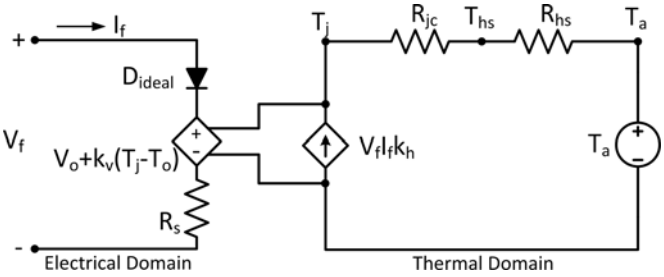

Fig. 1. Electrothermal equivalent circuit of one LED disposed on a heat sink.

$$T_{\rm hs} = T_a + nR_{\rm hs}V_f I_f k_h \tag{2}$$

$$T_j = T_a + R_{\rm ja}V_f I_f k_h \tag{3}$$

$$V_f(I_f, T_a) = \frac{V_o + R_s I_f + k_v(T_a - T_o)}{1 - I_f k_h k_v R_{\rm ja}}. \tag{4}$$

LEDs are known to produce a luminous flux that increases monotonically with forward current and decreases monotonically with junction temperature. Both these influences of I_f and T_j in the luminous flux (F) of LEDs can be modeled with an acceptable accuracy by two independent linear extrapolations [22]. Equations (5) and (6) model this behavior, in which c_0, c_1, d_0, and d_1 are the coefficients that arise from linear fitting of the normalized characteristics curves given by the LEDs' datasheet. Equation (5) is obtained under a constant reference current I_o, whereas (6) is obtained under a constant reference temperature T_o. At both $I_f = I_o$ and $T_j = T_o$, the LED yields its nominal luminous flux F_o (i.e., $F_T = F_I = 1$ p.u.)

$$F_T(T_j) = c_0 + c_1 T_j \tag{5}$$

$$F_I(I_f) = d_0 + d_1 I_f. \tag{6}$$

Multiplying (5) by (6) and adding the temperature effects modeled by (3) as well as the electrical model given in (4), it is possible to obtain the equation describing the static

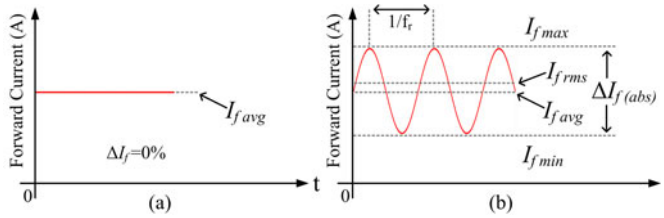

Fig. 2. Forward current waveforms: (a) pure dc current without a ripple and (b) dc current with superposed ac low-frequency ripple.

luminous flux of the LED module composed of *n* identical LEDs arranged over the same heat sink, as stated by (7). This static flux equation assumes thermal steady-state operation. Therefore, it is unsuitable for analyzing the photometrical impact of periodical changes in forward current around a given average current I_f, such as the ripple coming from an

$$\begin{aligned} &F_{\text{static}}(T_j, I_f) = nF_oF_T(T_j)F_I(I_f) \\ &= nF_o(c_0 + c_1T_j)(d_0 + d_1I_f) \\ &= \left\{ \begin{array}{l} nF_o \\ \quad \times\left[1+c_1\left(T_a + R_{ja}k_h\dfrac{I_f}{I_o}\dfrac{V_o + R_s\frac{I_f}{I_o} + k_v(T_a - T_o)}{1 - \frac{I_f}{I_o}k_hk_vR_{ja}}\right)\right. \\ \quad \left.-T_o\right] \\ \quad \times\left[d_1\dfrac{I_f}{I_o}\right] \end{array} \right\} \end{aligned} \tag{7}$$

ac–dc conversion in offline LED drivers. In the following section, a methodology based on dynamic photoelectrothermal modeling is proposed to analyze the dynamical flux regarding flicker generation, luminous performance degradation, and thermal behavior when 120 Hz current ripple is present.

III. Dynamical Photoelectrothermal Model

The static behavior presented in the previous section is a result of feeding the LEDs with a plain dc forward current I_f as shown in Fig. 2(a), for which thermal steady state is assumed at each point of the curve. However, as stated before, when a sinusoidal current ripple of frequency (f_r) is present due to the effect of the ac–dc conversion, the time-varying forward current waveform that must be considered is the one shown in Fig. 2(b). For the typical case of an offline LED driver, f_r is usually twice the line frequency; e.g., for 60 Hz mains, $f_r = 120$ Hz [16], [18]. Assessing the photometrical behavior of the LED system taking into account this effect demands for a dynamical analysis, which is named as such because there exists a time-varying current through the LEDs being driven.

This time-varying current can be mathematically described as function of time by (8), having an absolute peak-to-peak amplitude (in amperes) defined by (9), where $I_{f\max}$ is the peak LED current and $I_{f\min}$ is the minimum LED current. The per-unit ratio of current ripple to the average current will be, therefore, given by (10). Assuming a purely sinusoidal ripple, the RMS value of the ripple current will be (11)

$$i_f(t) = I_{f\,\text{avg}} + \frac{\Delta I_{f(\text{abs})}}{2}\sin(2\pi f_r t) \tag{8}$$

$$\Delta I_{f(\text{abs})} = (I_{f\max} - I_{f\min}) \tag{9}$$

$$\Delta I_{f(\text{pu})} = \frac{\Delta I_{f(\text{abs})}}{I_{f\,\text{avg}}} = \frac{(I_{f\max} - I_{f\min})}{I_{f\,\text{avg}}} \tag{10}$$

$$\begin{aligned} I_{f\,\text{rms}} &= \sqrt{\left(\frac{\Delta I_{f(\text{abs})}}{2\sqrt{2}}\right)^2 + {I_{f\,\text{avg}}}^2} \\ &= \sqrt{\frac{(I_{f\max} - I_{f\min})^2}{8{I_{f\,\text{avg}}}^2} + {I_{f\,\text{avg}}}^2}. \end{aligned} \tag{11}$$

Equation (7) may be modified to include the current dynamic behavior by using the $I_{f\text{rms}}$ for calculating the LED power and the current description in time given by (8), thus obtaining (12). This equation represents the dynamical behavior of luminous flux considering both electrical and thermal effects. However, it must be noticed that the time dependence is added only to the term referring to the LED electrical behavior, because it contains the fast portion of the LED dynamical response, which describes the electrical-to-optical conversion (several tens of nanoseconds in LEDs [20]), which may indeed be perceived as flicker [28].

On the other hand, the RMS forward current ($I_{f\text{rms}}$) accounts for the power dissipation in the LED system, thus directly affects the thermal term of the equation, which contains the slow dynamics of the system. The slow dynamic is a characteristic of the thermal subsystem, because temperature changes require the heating or cooling of a large amount of heat sink material. This fact relates the electrical effects in dynamical flux directly to the instantaneous current ($i_f\ (t)$), whereas the thermal effects are associated with the effective magnitude of these changes in current (i.e., $I_{f\text{rms}}$)

$$\begin{aligned} &F_{\text{dyn}}(i_f(t)) = nF_o \\ &\times\left[c_0+c_1\left(T_a + R_{\text{ja}}\frac{I_{f\,\text{rms}}}{I_o}k_h\frac{V_o + R_s\frac{I_{f\,\text{rms}}}{I_o} + k_v(T_a - T_o)}{1 - \frac{I_{f\,\text{rms}}}{I_o}k_hk_vR_{\text{ja}}}\right)\right] \\ &\times\left[d_0 + d_1\frac{i_f(t)}{I_o}\right]. \end{aligned} \tag{12}$$

The cyclical variation of luminous flux (and also luminance and illuminance) in time is usually known as flicker [5], [6]. The formula for calculating flicker percentage ($Fck_{\%}$) more commonly found in the literature is the Michelson contrast equation [28], given by (13), in which $E_{\max}$ is the maximum instantaneous illuminance and $E_{\min}$ is the minimum instantaneous illuminance.

From (12), it is possible to estimate the perceived flicker, which is proportional to the modulation in luminous flux due to current ripple ($E_{\max}$ and $E_{\min}$ can be considered scalars of $F_{\text{dyn}}(I_{f\max})$ and $F_{\text{dyn}}(I_{f\min})$, respectively, for flicker estimation purposes). Furthermore, (12) considers the junction temperature resulting from thermal design (R_{jc} and R_{hs}); thus, the thermal impacts in luminous flux are taken into account for

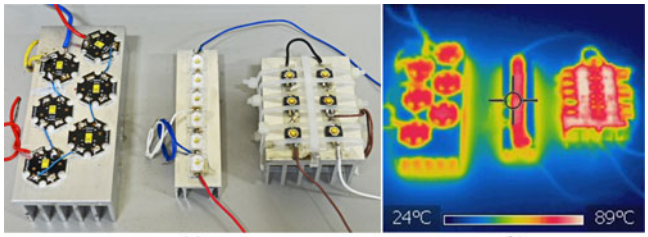

Fig. 3. Three LED modules experimentally analyzed: (a) modules A, B, and C and (b) thermal image at their respective design (I_N) current (all from left to right).

flicker estimation. Depending on the selected heat sink being used, the operating point changes and, consequently, the light output of the LEDs will present a predictable variation

$$Fck_{\%} = \frac{E_{\max} - E_{\min}}{E_{\max} + E_{\min}} 100\% = \frac{F_{\rm dyn}(I_{f\,\max}) - F_{\rm dyn}(I_{f\,\min})}{F_{\rm dyn}(I_{f\,\max}) + F_{\rm dyn}(I_{f\,\min})} 100\%. \quad (13)$$

IV. Experimental Setup and Data

In order to validate the proposed model, a laboratory setup has been developed. Three laboratory prototypes, denoted as A, B, and C, were built by using LEDs from Lumileds and Osram. Different ambient temperature and rated current were assumed for each module, thus attaining three completely different static characteristics and operating points to be studied. Each prototype consists of six devices in series assembled on heat sinks with different shapes and thermal resistances, as shown in Fig. 3. The characterization of each LED model was performed by linear regression of the curves—$V_f \times I_f$; $F \times I_f$; $F \times T_j$—provided by their respective datasheets [29]–[31]. All the data required by the model that were obtained from the datasheets together with the regression coefficients for expressions (5) and (6) are given in Table I. Also, in Table I, the statistical coefficients of determination for all linear regressions are presented: R_V^2 for the current versus voltage curve; R_T^2 for temperature correlation with luminous flux; and R_I^2 for current correlation with luminous flux. These coefficients indicate how well the data match the linearization curves. For all three regressions, in all three LED modules, R^2 was within 3% of a perfect linear fit (i.e., $R^2 = 1$) for the regions provided in the datasheets.

The main objective of the proposed model is to verify the LED photometrical behavior operating in different thermal and electrical conditions. For this purpose, two setups were assembled (see Figs. 4 and 5). A setup including a 40″ (1 m) integrating sphere (LMS400 by Labsphere) plus spectrophotometer (CDS2100 by Labsphere) (see Fig. 4) was used in the measurement of static quantities such as luminous flux, luminous efficacy, color coordinates, spectral distribution, and for assessment of the performance degradation of the LEDs static parameters when ripple is present. Another setup comprising a black box plus photodiodes (see Fig. 5) is used for measurement of

TABLE I
Parameters of the LEDs Tested

Parameter	LED module LED A	LED B	LED C
Manufacturer	Lumileds	OSRAM	Lumileds
Part number	LXML-PWN1	LUW-W5PM	LXK2-PWC4
n	6	6	6
$\mathbf{V}_o\,(\mathrm{V})$	2.7334	2.96	3.029
$R_s\,(\Omega)$	0.6640	0.7	0.589
R_V^2	0.9851	0.9838	0.9979
$\boldsymbol{k}_v\,(\mathbf{V}/^\circ\mathbf{C})$	−0.002	−0.003	−0.028
$\boldsymbol{k}_h$ [1]	0.85	0.75	0.80
$F_o\,(\mathrm{lm})$	100	106	105
$I_o\,(\mathrm{A})$	0.35	0.35	0.35
$I_{f\,\mathrm{avg}}\,(\mathrm{A})$	0.7	0.35	0.5
$f_r\,(\mathrm{Hz})$	120	120	120
$R_{\mathrm{jc}}\,(^\circ\mathrm{C/W})$	10	6.5	5.5
$R_{\mathrm{hs}}\,(^\circ\mathrm{C/W})$	4.39	11.73	5.8
c_0	1.0446	1.0260	1.0746
$c_1\,(^\circ\mathrm{C}^{-1})$	−0.0016	−0.0021	−0.0024
d_0	0	0	0
$d_1\,(\mathrm{A}^{-1})$	1.9642	1.24	0.872
$R^2{}_T$	0.9933	0.9672	0.9927
$R^2{}_I$	0.9868	0.9912	0.9792
$T_o\,(^\circ\mathrm{C})$	25	25	25
$T_a\,(^\circ\mathrm{C})$	25	35	30
$T_{j\,\max}\,(^\circ\mathrm{C})$	150	135	150

[1] Values for k_h were calculated using the measured LED radiant power.

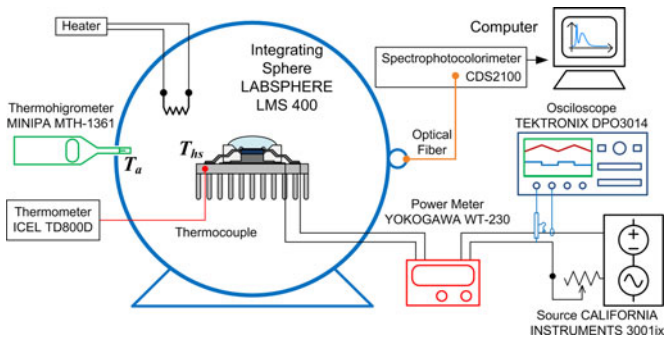

Fig. 4. Experimental setup for evaluating the impact of largely rippled currents on the LEDs photometric parameters (for the first and second experiments).

dynamical quantities such as flicker (i.e., instantaneous illuminance and its modulation).

The measurements were taken in a controlled environment, using a heater inside the experimental apparatus to keep a constant ambient temperature for the modules. A specific ambient temperature was used for each tested module (T_a, given in Table I). The LED module under test was inserted into the integrating sphere or black box, and a tightly controlled forward current was applied, both with and without the 120 Hz ripple. Measurements were taken after thermal steady-state conditions, i.e., when the heat sink temperature has been verified to be stabilized (45, 28, and 36 min, for modules A, B, and C, respectively).

The first test consisted of taking the static characteristic of the LED modules, without ripple, similarly to what was done in [22]. Both luminous flux and efficacy were measured, along with heat sink and ambient temperature (this last was kept constant at the specified T_a for each LED module).

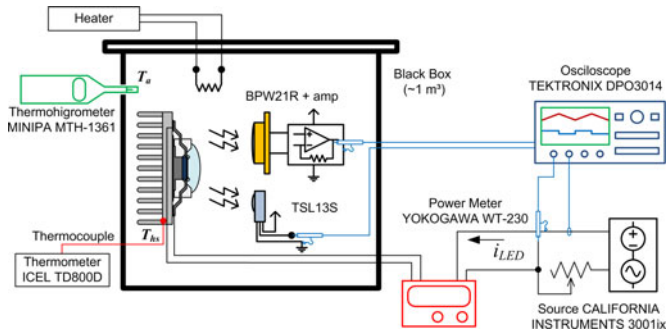

Fig. 5. Experimental setup for evaluating the impact of largely rippled currents on the LEDs dynamical performance (for the third and fourth experiments).

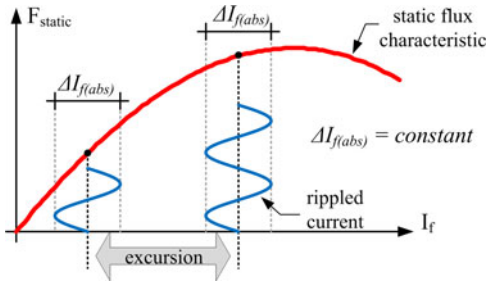

Fig. 6. Test of the excursion of the operating point of the module regarding flicker generation using a constant ripple amplitude (fourth experiment).

The second test analyzed the impact on the luminous flux and efficacy when increasing the current ripple through the LEDs. The average current through each module was kept constant at specified $I_{f\mathrm{avg}}$ while the ripple percentage was increased from 0% (no ripple) to 100% ($\Delta I_{f(\mathrm{abs})} = I_{f\mathrm{avg}}$).

While the first two tests were accomplished with the integrating sphere, the third one was performed inside the black box. This third experiment consisted of measuring the instantaneous illuminance (with photodiodes) of each module when fed with rippled currents, thus enabling the calculation of the generated flicker, according to the Michelson equation (13).

The fourth and last test analyzed the flicker generation as a function of the operating point of the LED module (i.e., the average forward current chosen as the rated current of the module, $I_{f\mathrm{avg}}$). In this test, a constant absolute current ripple amplitude ($\Delta I_{f(\mathrm{abs})}$) was applied to the LEDs and the average current was gradually increased, as shown in Fig. 6, thus testing the excursion of the operating point of the module. One hypothesis to be verified, proposed by Hui *et al.* [32] and [33], is that the closer to the peak of the static flux curve the operating point, the smaller the percentage flicker.

The static characteristics of all three LED models are shown in Fig. 7 regarding luminous flux and luminous efficacy (first experiment). The rise in heat sink temperature with increasing current is also shown for each module in Fig. 8. Both these curves regard the static characterization, because no ripple is yet present in current. The mean percentage error of experimental data with respect to the theoretical predictions for flux and heat sink temperature was calculated in each case and is also indicated in Figs. 7 and 8 for reference. For luminous flux, the mean error values were 2%, 1.5% and –8.4% for modules A, B, and C, respectively.

The theoretical prediction according to the photoelectrothermal static equation (7), along with the experimental data points, is plotted altogether. Overall luminous efficacy is calculated and predicted by dividing the luminous flux by the electrical power at each data point. The heat sinks were designed so as to yield close to maximum luminous flux with the specified nominal current ($I_f = I_{f\mathrm{avg}}$).

The static flux and efficacy curves show a fairly good agreement between experimental data and theoretical prediction. The small deviations can be attributed to some of the simplifying assumptions: 1) all devices of a particular model are rigorously identical; 2) the flux versus forward current and flux versus temperature relationships are perfectly linear; and 3) the thermal resistance of the LED–heat sink interface is neglected for analysis. Nevertheless, these curves provide important insights into the design of the thermal and electrical specifications of LED-based lighting systems, with limited but sufficient accuracy.

When a current ripple is superimposed to the nominal value of current (i.e., the rated design current of the module) and its amplitude is continuously increased (second experiment), it is possible to measure the performance degradation, as depicted in the experimental curves of Fig. 9; with increasing ripple, both the flux and the efficacy of the module decrease. In these curves, the 100% values of flux and efficacy are defined as those at $I_f = I_{f\mathrm{avg}}$ and $\Delta I_{f(\mathrm{abs})} = 0$.

The decrements in luminous flux and efficacy get more accentuated for ripples above $\Delta I_{f(\%)} = 50\%$ for modules B and C. At 50%, the degradation may be considered still quite negligible for all modules. This behavior has already been reported in [19] as an argument for using a 50% ripple in current as the upper limit in the design of offline LED drivers, thus enabling capacitor size reduction. As a remark, similar flux and efficacy decreasing rates were also observed for other operating points (e.g., for 50% of the rated current of the modules), thus suggesting that this behavior is mostly related to the increase in the ripple amplitude and not to operating the LEDs close to flux saturation in the static curve; in [17], a similar experiment was performed with an LED module that was not operated at the peak of the saturation of the curve (e.g., with an oversized heat sink), and the resulting behavior of flux and efficacy drop was also very similar. Table II compares all three LEDs regarding the flux and efficacy depreciations for three main cases: 30% (small ripple), 50% (intermediate ripple), and 80% (large ripple). This comparison shows that for both 30% and 50% ripple, the performance degradation is mainly negligible, while at 80% the drop in luminous flux and efficacy is already accentuated.

The normalized spectral power distributions (SPDs) of the LED modules for zero ripple are also static characteristics; they are shown in Fig. 10 (continuous black lines). They show the typical emission spectrum of each module at their nominal current. The CCT values indicated in this figure were measured and classified according to the tolerance quadrants given in the ANSI C78.377 standard [34]. Fig. 10 also shows the measured

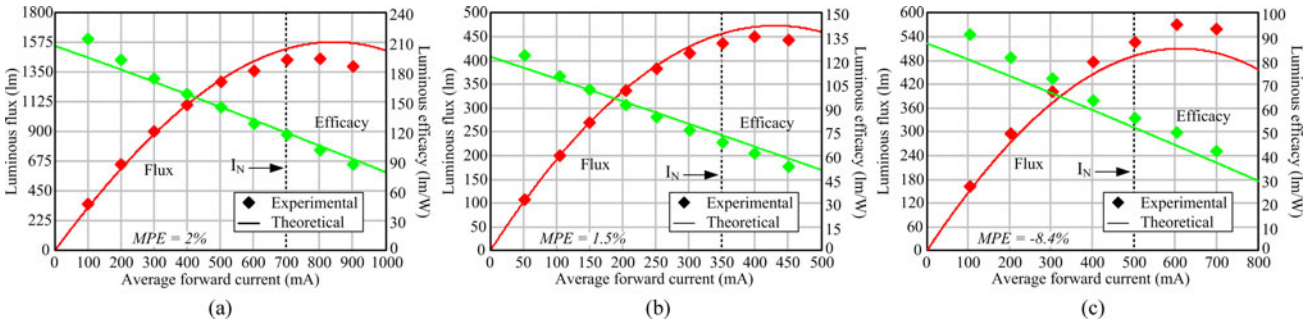

Fig. 7. First experiment: static characterization of the LED modules regarding luminous flux and luminous efficacy for (a) module A, (b) module B, and (c) module C.

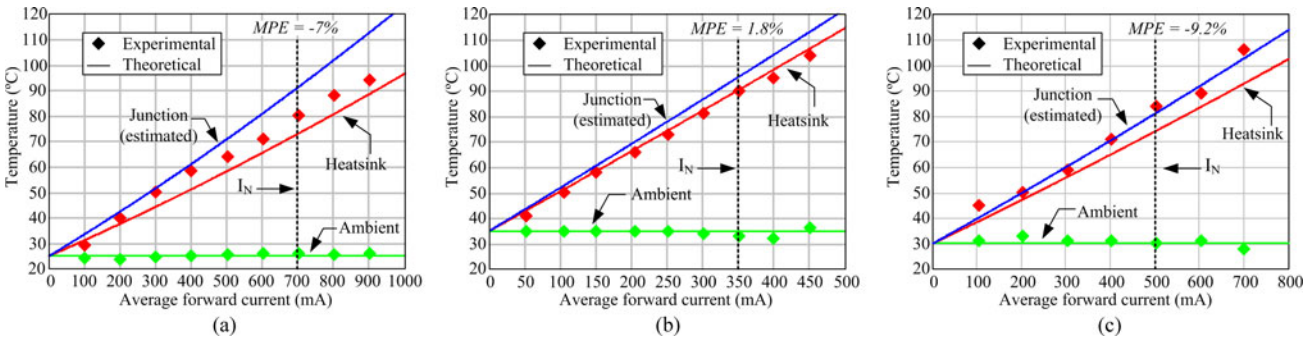

Fig. 8. First experiment: static characterization of the LED modules regarding heat sink and ambient temperatures for (a) module A, (b) module B, and (c) module C.

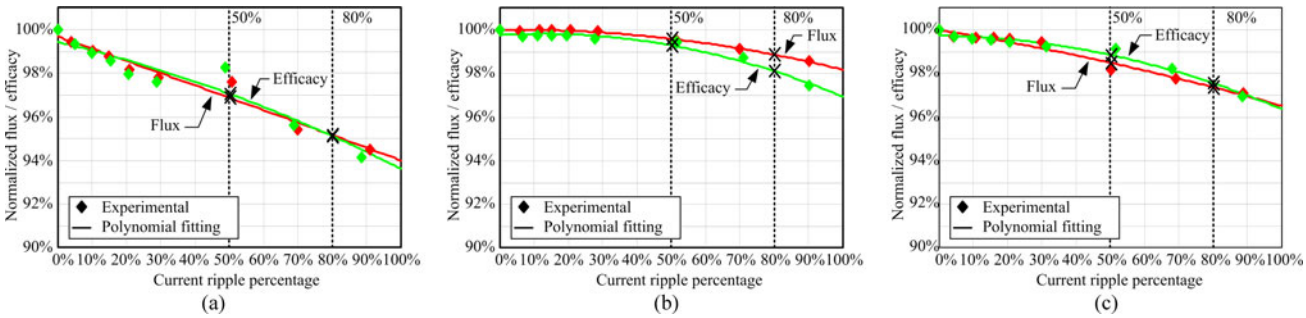

Fig. 9. Second experiment: degradation of the light output and efficacy when ripple is present superposed to the nominal average current in (a) module A, (b) module B, and (c) module C.

TABLE II
COMPARISON OF LUMINOUS PERFORMANCE DEGRADATION
(SECOND EXPERIMENT)

LED A I_N = 700 mA	**Ripple**	**30%**	**50%**	**80%**
	Normalized flux	98%	96.9%	95.1%
	Normalized efficacy	98.1%	97%	95.1%
LED B I_N = 350 mA	**Ripple**	**30%**	**50%**	**80%**
	Normalized flux	99.9%	99.6%	98.8%
	Normalized efficacy	99.7%	99.3%	98%
LED C I_N = 500 mA	**Ripple**	**30%**	**50%**	**80%**
	Normalized flux	99.1%	98.5%	97.3%
	Normalized efficacy	99.4%	98.8%	97.5%

normalized SPDs of the modules when 50% and 90% ripple is present (dashed blue and green lines). These spectra show a slight overall reduction in spectral power, with the arrows pointing to trends observed in the chromatic shifts (at the peak of blue LED emission and at the peak of the YAG:Ce phosphor emission).

In order to analyze the chromatic deviation resulting from increasing the current ripple, the CIE 1931 *xy* chromaticity coordinates were obtained for the same data points shown in Fig. 9 (from 0% to 90% ripple), for all three modules. These coordinates are plotted in Fig. 11, with a linear trend showing the direction of the chromatic dislocation. It can be seen that in all three cases there is a color shift toward blue in the *xy* chromaticity chart, meaning that the LEDs tend to become bluish-white when the ripple is increased. For quantitatively analyzing this issue, the color difference equation for the CIELAB color space

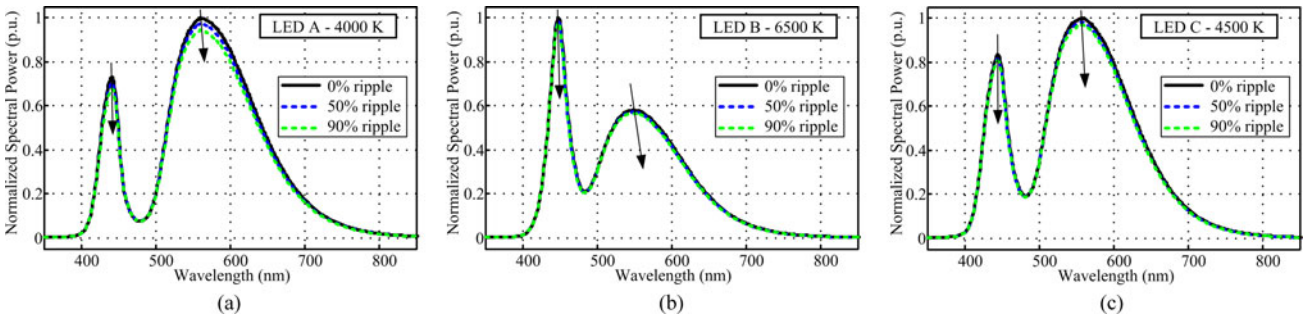

Fig. 10. Spectra of the three modules under nominal operation with no ripple (continuous line, static spectral characteristic) and for 50% and 90% ripple in current (dashed lines). Results are also from the first and second experiments.

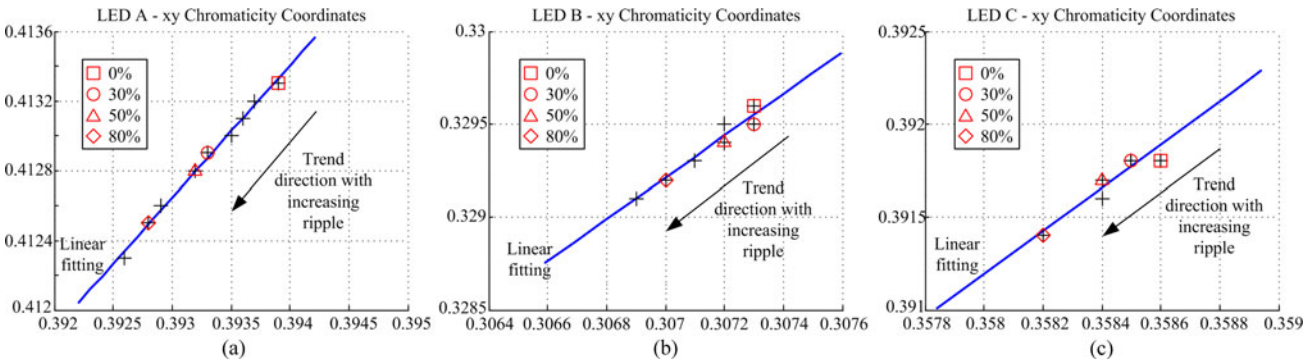

Fig. 11. Chromaticity coordinates for (a) module A, (b) module B, and (c) module C at all ripple data points analyzed (some points are superposed because no changes in chromaticity coordinates were detected between two given adjacent tests). Points of interest are indicated by the legend. Results are also from the first and second experiments.

TABLE III
COMPARISON OF COLOR DIFFERENCES IN RELATION TO 0% RIPPLE

LED A	**Ripple**	**50%**	**90%**
	ΔE^*_{ab}	2.6	5.3
LED B	**Ripple**	**50%**	**90%**
	ΔE^*_{ab}	0.99	1.6
LED C	**Ripple**	**50%**	**90%**
	ΔE^*_{ab}	1.3	2.3

[35] was used to calculate color distance ΔE^*_{ab} between the chromaticity coordinates at 0% ripple and at two other test points: 50% (a point of overall interest in this study) and 90% (maximum tested ripple). The *xy* chromaticity coordinates plus the luminous flux were used to find the *XYZ* tristimulus values and then convert them to Lab coordinates, using the CIE D65 illuminant as the reference white point for the CIELAB color space. The values found for color difference ΔE^*_{ab} are given in Table III. According to [36], the just-noticeable color difference threshold for ΔE^*_{ab} can be up to 2.56. At 50% ripple, it can be considered that all LEDs present unnoticeable color difference from a 0% ripple (although LED A presents a color change very slightly above the 2.56 threshold). Even at 90% ripple (the highest ripple used in all tests), the color difference is below the threshold for LEDs B and C, whereas LED A was the only one presenting color change above the established limit.

Figs. 12 and 13 show the results obtained from illuminance measurements done with the photodiodes inside the black box

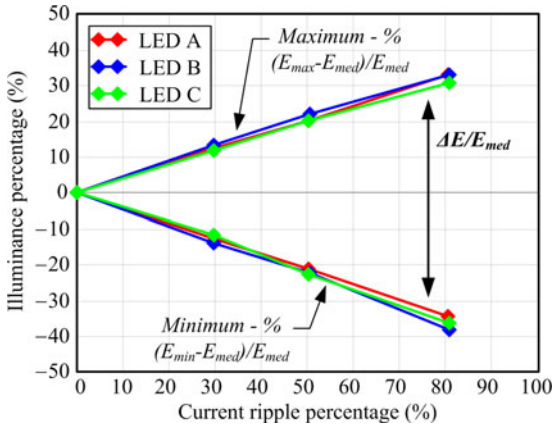

Fig. 12. Third experiment: maximums and minimums of the illuminance variation (flicker), plotted together for modules A, B, and C for various percentage values of current ripple.

for all three of the LED modules (third experiment). For ease of comparison, all values were normalized with respect to the average illuminance in Fig. 12, whereas the flicker shown in Fig. 13 (as defined by the Michelson equation) is already a percentage quantity. These results show that flicker varies linearly with the current ripple percentage. Furthermore, the transference of current variation (i.e., ripple) to flux variation (i.e., flicker) decreases slightly with an increase in ripple amplitude. For

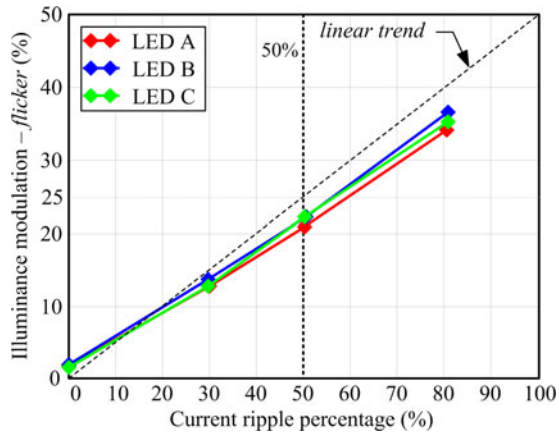

Fig. 13. Third experiment: flicker calculated from Michelson contrast equation measured for various percentage values of current ripple, showing a linear trend.

example, a 30% ripple causes ca. 15% flicker, whereas an 80% ripple causes ca. 35% flicker instead of 40%. This photometrical effect cannot be entirely predicted after (12), but represents only a very slight deviation from the calculation, appearing only at very large ripples. Some oscilloscope waveforms are given in Fig. 14 for three test points (30%, 50%, and 80% ripple), showing the measurement of illuminance modulation in time for module A.

Fig. 15 shows the test results of excursion of the operating point of each module when adopting an absolute ripple ($\Delta I_{f(\mathrm{abs})}$) of 200, 105, and 180 mA for modules A, B, and C, respectively (fourth experiment). These values yield a relative ripple close to 30% for all three modules. Theoretical prediction is also provided, since it can be obtained from the dynamical flux equation (12) combined with the Michelson equation (13).

The results shown in Fig. 15 indicate that the overall flicker reduces with an increase in the average value of I_f. This is mostly because the average flux increases (excursion in the static characteristic) but the amplitude of the dynamical luminous flux does not increase at the same rate. Therefore, flicker does not increase at the same rate as the average luminous flux when the average current at the operating point is increased. This leads to the conclusion that the point where luminous flux is maximal and where the static curve saturates is not actually a point of minimum flicker transference. Nevertheless, it can be stated that the flicker beyond a certain point can be considered small enough taking into account the human perception of stroboscopic effects [6]. The hypothesis that such a minimum flicker point existed, made before in [32] and [33], assumed thermal steady-state operation at all points of the curve, which cannot be applied for fast periodical current oscillations (such as ripple). This means that flicker cannot be calculated by simply reflecting the varying current directly in the static flux curve, because each point is a point of thermal steady state. However, by using (12), flicker can be correctly calculated because only the fast-responding part of the photoelectrothermal model is assumed to be time varying (i.e., flux versus current characteristic). The findings in this paper contrast with the hypothesis proposed by

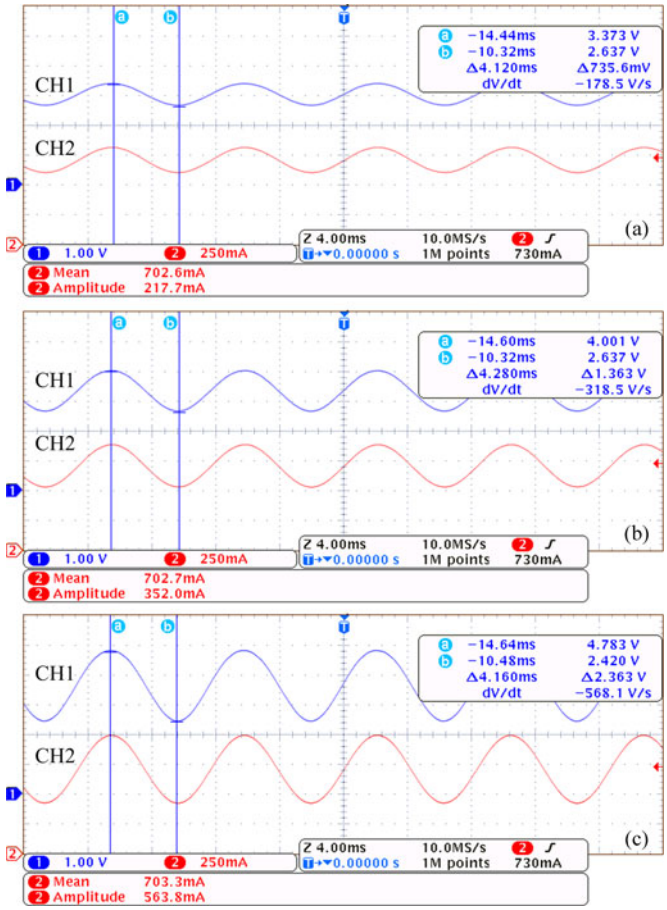

Fig. 14. Waveforms obtained during flicker measurement (third and fourth experiments) of module A: CH1 (1 V/div)—output of the photodiode circuit (TSL13S sensor), CH2 (250 mA/div)—LED module current, for (a) 30%, (b) 50%, and (c) 80% current ripple. Horizontal scale: 4 ms/div.

Hui *et al.* [32] and [33] that, at the saturation of the static curve (maximum flux), the flicker will be minimum, which had not been experimentally verified in such works.

V. Conclusion

This paper presented the study of the LED photometrical behavior considering the electrothermal methodology, which is modified to include the effects of current ripple, thus allowing for predictions of flickering of the light output at low frequency (120 Hz in this case studied).

A theoretical approach was performed considering the luminous flux behavior as a function of the forward current and temperature. The luminous flux was characterized in static (stiff dc current and at thermal steady state) and dynamical (at a given operating point with some current ripple superposed) forms.

Three different heat sinks were used in this study, thus yielding three LED modules (A, B, and C) with completely different static characteristics. Nevertheless, all three modules were subjected to the same tests, under a dynamical analysis, to enable extracting meaningful results of LED systems performance and behavior when they are subjected to sinusoidal current ripple. Experimental results indicate that there may be

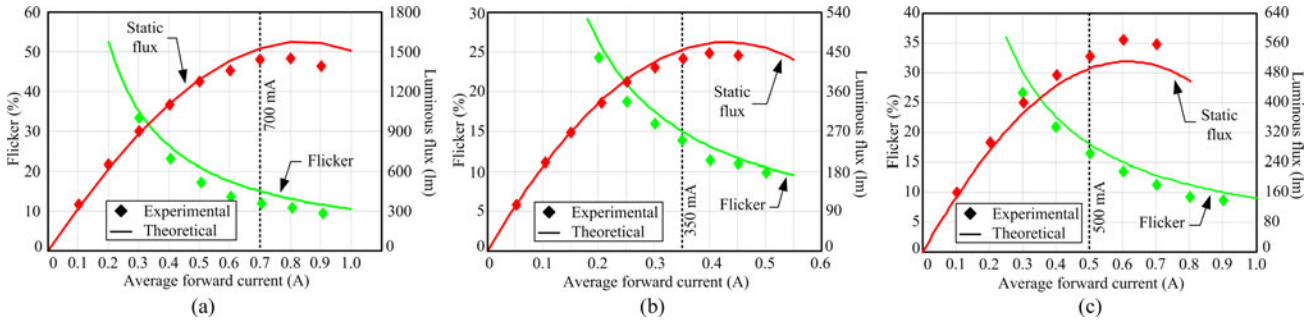

Fig. 15. Fourth experiment: test of excursion of operating point: flicker as function of the average current for a constant absolute ripple amplitude in modules (a) A (ripple 200 mA), (b) B (ripple 105 mA), and (c) C (ripple 180 mA).

some points of operation (i.e., average design current values) that are better suited for the LED system considering not only the maximum luminous flux but also its dynamic behavior—e.g., the flicker yielded or the luminous performance degradation due to the inherent current ripple that the driver converter may impose. In these hypothesized close-to-optimum operating points, both minimal capacitance requirements and low enough LED flickering can be found for a given driving converter design.

For example, it is possible to minimize the nominal current of the LED module and maximize the current ripple, while staying within safe margin for the flicker yielded—both of these fine-tuning actions would reduce capacitance requirements.

This hypothesis also leads to the conclusion that designing the LED module to operate at the peak of the static flux versus current curve (i.e., at saturation) may not be the best choice for all cases, since it only maximizes the luminous flux. The flicker yielded is not a function of the excursion of a rippled current in the static curve, but a function of the dynamical flux behavior modeled in this paper. This mathematical approach has been shown to be in good agreement with the measurements performed with three different heat sinks bearing three different LED models, for which also different operating conditions were designed and employed (nominal average current and ambient temperature of all three modules are different).

The theoretical prediction and the experimental results presented in this study show that, in spite of a relatively high current ripple (e.g., as high as 50%), the resulting flicker is acceptable and performance degradation of the LEDs is small, depending on the good choice of a combination of both heat sink and operating current. This makes it possible the use of smaller capacitances in LED drivers, thus linking both the LED module design (heat sink, LED model, number of LEDs, etc.) and the driver design (operating current, amount of current ripple at the output, output voltage, etc.). The use of smaller filter capacitances in LED drivers provides cost and volume reduction, and it also enables the use of other capacitor technologies with a higher lifespan than that of electrolytic capacitors (such as film capacitors); thus, the whole LED system lifespan and reliability may benefit.

The most relevant contributions of this study are those providing several guidelines that can be used for future LED driver design and implementation. Using the experimental evidence compiled in this study, it has been proven that for a 50% current ripple the following facts apply:

1) The drops in both luminous flux and luminous efficacy are below 3% for all LEDs.
2) The chromatic deviation of the LEDs (ΔE^*_{ab}, calculated from measurements) is within the established threshold for human color difference noticeability.
3) The yielded flicker, as defined by the Michelson equation, remained below 25% for all LEDs. This value is also within acceptable limits of flicker and perception of stroboscopic effects., because according to the specialized literature [6], subjects under test found effects from 100 to 120 Hz flicker "acceptable" up until 25–30% illuminance modulation. Also, PAR1789 standard [7] states that the modulation threshold above which headaches can be induced is 35%, at 100 Hz. Moreover, in [37], it is stated that stroboscopic effects could only be noticed for modulations exceeding 30%, and under some very specific circumstances.

REFERENCES

[1] E. F. Schubert, *Light-Emitting Diodes*, 1st ed. New York, NY, USA: Cambridge Univ. Press, 2003.
[2] J. Y. Tsao, "Solid-state lighting: Lamps, chips, and materials for tomorrow," *IEEE Circuits Devices Mag.*, vol. 20, no. 3, pp. 28–37, May/Jun. 2004.
[3] C. R. B. S. Rodrigues, P. S. Almeida, G. M. Soares, J. M. Jorge, D. P. Pinto, and H. A. C. Braga, "An experimental comparison between different technologies arising for public lighting: LED luminaires replacing high pressure sodium lamps," in Proc. IEEE Int. Symp. Ind. Electron., 2011, pp. 141–146.
[4] Y. K. Cheng and K. W. E. Cheng, "General Study for using LED to replace traditional lighting devices," in *Proc. 2nd Int. Conf. Power Electron. Syst. Appl.*, 2006, pp. 173–177.
[5] *The IESNA Lighting Handbook*, IESNA, New York, NY, USA, 9th ed., 2000.
[6] J. D. Bullough, K. Sweater Hickcox, T. R. Lein, A. Lok, and N. Narendran, "Detection and acceptability of stroboscopic effects from flicker," *Lighting Res. Technol.*, vol. 44, no. 4, pp. 477–483, Dec. 2012.
[7] A. Wilkins, J. Veitch, and B. Lehman, "LED lighting flicker and potential health concerns: IEEE standard PAR1789 update," in *Proc. IEEE Energy Convers. Congr. Expo.*, 2010, pp. 171–178.
[8] A. J. Wilkins, *Visual Stress*. New York, NY, USA: Oxford Univ. Press, 1995.
[9] D. S. G. Samuel, M. Berman, I. L. Bailey, R. D. Clear, and T. W. Raasch, "Human electroretinogram responses to video displays, fluorescent

lighting, and other high frequency sources," *Optometry Vis. Sci.*, vol. 68, pp. 645–662, 1991.
[10] P. S. Almeida, F. J. Nogueira, L. Guedes, and H. A. C. Braga, "An experimental study on the photometrical impacts of several current waveforms on power white LEDs," in *Proc. Brazilian Power Electron. Conf.*, 2011, pp. 728–733.
[11] H. Chen and S. Y. R. Hui, "Dynamic prediction of correlated color temperature and color rendering index of phosphor-coated white light-emitting diodes," *IEEE Trans. Ind. Electron.*, vol. 61, no. 2, pp. 784–797, Feb. 2014.
[12] T. Xuehui and S. Y. R. Hui, "Dynamic photoelectrothermal theory for light-emitting diode systems," *IEEE Trans. Ind. Electron.*, vol. 59, no. 4, pp. 1751–1759, Apr. 2012.
[13] J. M. Alonso, D. Gacio, A. J. Calleja, F. Sichirollo, M. F. da Silva, M. A. D. Costa, and R. N. do Prado, "Reducing storage capacitance in off-line LED power supplies by using integrated converters," in *Proc. IEEE Ind. Appl. Soc. Annu. Meeting*, 2012, pp. 1–8.
[14] Y. X. Qin, H. S. H. Chung, D. Y. Lin, and S. Y. R. Hui, "Current source ballast for high power lighting emitting diodes without electrolytic capacitor," in *Proc. 34th Conf. IEEE Ind. Electron.*, 2008, pp. 1968–1973.
[15] M. Arias, D. G. Lamar, J. Sebastian, D. Balocco, and A. A. Diallo, "High-efficiency LED driver without electrolytic capacitor for street lighting," *IEEE Trans. Ind. Appl.*, vol. 49, no. 1, pp. 127–137, Jan./Feb. 2013.
[16] J. M. Alonso, J. Vina, D. G. Vaquero, G. Martínez, and R. Osorio, "Analysis and design of the integrated double buck–boost converter as a high-power-factor driver for power-LED lamps," *IEEE Trans. Ind. Electron.*, vol. 59, no. 4, pp. 1689–1697, Apr. 2012.
[17] R. A. Pinto, M. R. Cosetin, J. G. Roncalio, M. Melo, T. B. Marchesan, M. A. Dalla Costa, and R. N. do Prado, "Street lighting system based on integrated buck-flyback converter to supply LEDs without energy consumption during the peak load time," in Proc. Brazilian Power Electron. Conf., 2011, pp. 891–897.
[18] P. S. Almeida, M. A. Dalla Costa, J. M. Alonso, and H. A. C. Braga, "Application of series resonant converters to reduce ripple transmission to LED arrays in offline drivers," *Electron. Lett.*, vol. 49, pp. 414–415, 2013.
[19] P. S. Almeida, G. M. Soares, D. P. Pinto, and H. A. C. Braga, "Integrated SEPIC buck-boost converter as an off-line LED driver without electrolytic capacitors," presented at the 38th Annual Conference on IEEE Industrial Electronics Society, Montreal, QC, Canada, 2012.
[20] T. Siew-Chong, "General n-level driving approach for improving electrical-to-optical energy-conversion efficiency of fast-response saturable lighting devices," *IEEE Trans. Ind. Electron.*, vol. 57, no. 4, pp. 1342–1353, Apr. 2010.
[21] S. Buso, G. Spiazzi, M. Meneghini, and G. Meneghesso, "Performance degradation of high-brightness light emitting diodes under DC and pulsed bias," *IEEE Trans. Device Mater. Rel.*, vol. 8, no. 2, pp. 312–322, Jun. 2008.
[22] V. C. Bender, O. Iaronka, W. D. Vizzotto, M. A. D. Costa, R. N. do Prado, and T. B. Marchesan, "Design methodology for light-emitting diode systems by considering an electrothermal model," *IEEE Trans. Electron Devices*, vol. 60, no. 11, pp. 3799–3806, Nov. 2013.
[23] C. Biber, "LED light emission as a function of thermal conditions," in *Proc. 24th Annu. IEEE Semicond. Therm. Meas. Manage. Symp.*, 2008, pp. 180–184.
[24] S. Y. Hui and Y. X. Qin, "A general photo-electro-thermal theory for light emitting diode (LED) systems," *IEEE Trans. Power Electron.*, vol. 24, no. 8, pp. 1967–1976, Aug. 2009.
[25] C. P. Wang, T. T. Chen, H. K. Fu, T. L. Chang, and P. T. Chou, "Transient analysis of partial thermal characteristics of multistructure power LEDs," *IEEE Trans. Electron Devices*, vol. 60, no. 5, pp. 1668–1672, May 2013.
[26] W. Biqing, L. Siqi, S. Tien-Mo, G. Yulin, L. Yijun, Z. Lihong, C. Guolong, and C. Zhong, "Junction-temperature determination in InGaN light-emitting diodes using reverse current method," *IEEE Trans. Electron Devices*, vol. 60, no. 1, pp. 241–245, Jan. 2013.
[27] T. Xuehui and Z. Dongli, "Thermal parameter extraction method for light-emitting diode (LED) systems," *IEEE Trans. Electron Devices*, vol. 60, no. 6, pp. 1931–1937, Jun. 2013.
[28] B. Lehman, A. Wilkins, S. Berman, M. Poplawski, and N. J. Miller, "Proposing measures of flicker in the low frequencies for lighting applications," in *Proc. IEEE Energy Conver. Congr. Expo.*, 2011, pp. 2865–2872.
[29] *Technical Datasheet DS64*, Philips Lumileds, San Jose, CA, USA, 2011.
[30] *Golden DRAGON oval Plus LUW W5PM*, Osram, Munich, Germany, 2010.
[31] *Technical Datasheet DS60*, Philips Lumileds, San Jose, CA, USA, 2007.
[32] C. K. Lee, S. Li, and S. Y. R. Hui, "A design methodology for smart LED lighting systems powered by weakly regulated renewable power grids," *IEEE Trans. Smart Grid*, vol. 2, no. 3, pp. 548–554, Sep. 2011.
[33] S. Y. R. Hui, H. T. Chen, and X. H. Tao, "An extended photoelectrothermal theory for LED systems: A tutorial from device characteristic to system design for general lighting," *IEEE Trans. Power Electron.*, vol. 27, no. 11, pp. 4571–4583, Nov. 2012.
[34] "American national standard for electric lamps—Specifications for the chromaticity of solid state lighting products," ANSI-NEMA-ANSLG-C78.377, 2008.
[35] B. Hill, T. Roger, and F. W. Vorhagen, "Comparative analysis of the quantization of color spaces on the basis of the CIELAB color-difference formula," *ACM Trans. Graph.*, vol. 16, pp. 109–154, 1997.
[36] M. Stokes, M. D. Fairchild, and R. S. Berns, "Precision requirements for digital color reproduction," *ACM Trans. Graph.*, vol. 11, pp. 406–422, 1992.
[37] J. Bullough, K. Sweater Hickcox, T. Klein, and N. Narendran, "Effects of flicker characteristics from solid-state lighting on detection, acceptability and comfort," *Lighting Res. Technol.*, vol. 43, pp. 337–348, Sep. 2011.

Pedro S. Almeida (S'09) was born in Cataguases, Brazil, in 1987. He received the B.S. and M.Sc. degrees in electrical engineering from the Federal University of Juiz de Fora (UFJF), Juiz de Fora, Brazil, in 2010 and 2012, respectively, where he is currently working toward the Ph.D. degree.

Since 2008, he has been a full-time Researcher with the Modern Lighting Research Group based at the Engineering School of UFJF. His main research interests include electronic power conversion, high power factor rectifiers and active power factor correction, solid-state lighting and LED driving, high- and low-pressure discharge lamps and high-frequency electronic ballasts, dimming, spectrophotometry, microcontrollers applied to power electronics, and the modeling and control of electronic power converters.

Mr. Almeida also serves as a Reviewer for international journals and conferences in the field of power electronics and electrical engineering.

Vitor C. Bender was born in Panambi, RS, Brazil, in 1987. He received the B.S. degree in electrical engineering in 2011 and the M.Sc. degree in 2012, both from the Federal University of Santa Maria, Santa Maria, Brazil, where he is currently working toward the Doctoral degree with the Electronic Ballast Research Group.

His research interests include lighting systems, electronic ballasts, LED and OLED drivers, LED and OLED modeling, and thermal design.

Henrique A. C. Braga (S'83–M'88–SM'01) received the B.S. degree in electrical engineering from the Federal University of Juiz de Fora (UFJF), Juiz de Fora, Brazil, in 1982, the master's degree in electrical engineering from COPPE/UFRJ, Rio de Janeiro, Brazil, in 1988, and the Doctor degree (Dr.Eng.) in the same field from the Federal University of Santa Catarina, INEP/UFSC, Florianópolis, Brazil, in 1996.

He has been teaching in the UFJF since 1985. He is currently an Associate Professor at UFJF, teaching in the undergraduate and postgraduate programs in electrical engineering, where he is mainly concerned with the subjects of basic electronics and power electronics. From 2005 to 2006, he attended a postdoctoral stage at the University of Oviedo in the Spanish city of Gijón, Asturias. He is involved in activities related to power electronics, efficient lighting and converters applied to renewable energy.

Dr. Braga is a Member of the Brazilian Power Electronics Society (SOBRAEP), serving as the Chair and Associate Editor of this scientific organization until 2015.

Marco A. Dalla Costa (S'03–M'09) was born in Santa Maria, Brazil, in 1978. He received the B.S. and M.Sc. degrees in electrical engineering from the Federal University of Santa Maria, Santa Maria, Brazil, in 2002 and 2004, respectively, and the Ph.D. degree (with hons.) in electrical engineering from the University of Oviedo, Gijón, Spain, in 2008.

From 2008 to 2009, he was an Associate Professor with the Universidade de Caxias do Sul, Brazil. Since 2009, he has been an Associate Professor at the Federal University of Santa Maria.

He is author of more than 30 journal papers and more than 60 international conference papers, and is holder of two Spanish patents. His research interests include dc/dc converters, power factor correction stages, dimming systems, high-frequency electronic ballasts, discharge-lamp modeling, electronic starters for high-intensity-discharge lamps, light-emitting-diode systems, renewable energy systems, and solid state transformers.

Dr. Dalla Costa also serves as Reviewer for several IEEE Journals and Conferences in the field of power electronics.

Tiago B. Marchesan (S'03–M'08) was born in Santa Maria, Brazil, in 1980. He received the B.S. (with first-class honors) and Ph.D. degrees in electrical engineering from the Federal University of Santa Maria (UFSM), Santa Maria, Brazil, in 2003 and 2008, respectively.

Since 2000, he has been a Researcher with the Electronic Ballast Research Group, UFSM. He was an Associate Professor with the Technology Department, Regional University of the Northwest, Rio Grande do Sul, Ijui, Brazil, during 2008. From 2009 to 2011, he was a Research and Development Engineer with the Power Transformer Group, WEG Electric Corporation, and a Professor with Sinos River Valley University, Rio Grande do Sul, São Leopoldo, Brazil. Since 2011, he has been a Full Professor with the UFSM. His research interests include electronic ballasts, high-intensity-discharge lamps, LEDs, dimming systems, and modeling and simulation of power converters.

J. Marcos Alonso (S'94–M'98–SM'03) received the M.Sc. and Ph.D. degrees from the University of Oviedo, Oviedo, Spain, in 1990 and 1994, respectively, both in electrical engineering.

Since 2007, he has been a Full Professor in the Electrical Engineering Department of the University of Oviedo. He is coauthor of more than three-hundred journal and conference publications. He was Supervisor of eight Ph.D. thesis and he is the holder of seven Spanish patents. He has participated in more than 50 research projects and contracts with companies. His research interests include electronic ballasts, LED power supplies, power factor correction, dc–dc converters, resonant inverters, and single-phase high frequency switching converters in general.

Dr. Alonso received the Early Career Award of the IEEE Industrial Electronics Society in 2006. He was honored with the University of Oviedo Electrical Engineering Doctorate Award for 1996. He also holds three IEEE paper awards. Since 2002, he has been serving as an Associate Editor of the IEEE TRANSACTIONS ON POWER ELECTRONICS. He has been a Co-Guest Editor of two special issues in lighting applications published in the IEEE TRANSACTIONS ON POWER ELECTRONICS (2007) and the IEEE TRANSACTIONS ON INDUSTRIAL ELECTRONICS (2012) and has co-organized several conference special sessions. He also serves as Secretary of the IEEE IAS Industrial Lighting and Display Committee. He has been elected as Member-at-Large of the IEEE IAS Executive Board for the term 2013–2014. He is also a member of the European Power Electronics Association and he belongs to the International Steering Committee of the European Conference on Power Electronics and Applications.